Cell-cycle-dependent phosphorylation of the nuclear pore Nup107–160 subcomplex

Joseph S. Glavy*, Andrew N. Krutchinsky†‡, Ileana M. Cristea†, Ian C. Berke*, Thomas Boehmer*, Günter Blobel*§, and Brian T. Chait†§

Laboratories of †Mass Spectrometry and Gaseous Ion Chemistry and *Cell Biology, Howard Hughes Medical Institute, The Rockefeller University, 1230 York Avenue, New York, NY 10021

Contributed by Günter Blobel, January 3, 2007 (sent for review December 10, 2006)

The nuclear pore complex (NPC) mediates macromolecular transport between the nucleus and the cytoplasm. Many NPC proteins (nucleoporins, Nups) are modified by phosphorylation. It is believed that phosphorylation regulates the breakdown of the nuclear envelope at mitosis and the disassembly of the NPC into different subcomplexes. In this study, we examined the cell-cycle-dependent phosphorylation of the Nup107–160 subcomplex, a core building block of the NPC. Using *in vivo* ^{32}P labeling in HeLa cells, we found that Nup107, Nup96, and Nup133 are phosphorylated during mitosis. To precisely map the phosphorylation sites within the complex, we used a comprehensive multiple-stage MS approach (MS, MS^2, and MS^3), establishing that Nup160, Nup133, Nup96, and Nup107 are all targets of phosphorylation. We determined that the phosphorylation sites are clustered mainly at the N-terminal regions of these proteins, which are predicted to be natively disordered. In addition, we determined the cell-cycle dependence of the phosphorylation of these sites by using stable isotope labeling and MS^2 analysis. Measurement of the site-specific phosphorylation ratios between mitotic and G_1 cells led us to conclude that several phosphorylation events of the subcomplex are mainly mitotic. Based on these results and our finding that the entire Nup107–160 subcomplex is stable throughout the cell cycle, we propose that phosphorylation does not affect interactions within the Nup107–160 subcomplex, but regulates the association of the subcomplex with the NPC and other proteins.

mitosis | nucleoporin | mass spectrometry | nuclear pore complex | mammalian

The nuclear pore complex (NPC) is the principal passageway for nucleocytoplasmic macromolecular traffic (1). It is composed of ≈30 proteins (2, 3), termed nucleoporins (Nups) that are organized into a pseudosymmetric structure with a 2-fold plane quasi-parallel to the nuclear envelope and an 8-fold axis of symmetry about the nucleo-cytoplasmic axis. Most of the Nups are part of a symmetric core structure and therefore likely occur in at least 16 copies per NPC (e.g., Nup107, Nup133) (2, 3).

Higher eukaryotic cells undergo an open mitosis, during which the NPC is disassembled into subcomplexes. Mitotic disassembly is thought to be triggered by phosphorylation (4–6). Interestingly, subcomplexes similar to those generated during mitosis can also be isolated by exposure of G_1 cells to treatment with the nonionic detergent Triton X-100 under physiological salt concentration (7). The best-characterized subcomplex is the vertebrate Nup107–160 and the homologous Nup84 subcomplex in *Saccharomyces cerevisiae*. The Nup107–160 subcomplex has nine members (Nup160, Nup133, Nup107, Nup96, Nup75, Nup43, Nup37, Seh1, and Sec 13) (8), whereas the Nup84 subcomplex has seven members (9).

In the "protocoatomer" hypothesis, the Nup107–160 subcomplex has been proposed to stabilize the sharp bend between the inner and outer nuclear envelope membrane (10). Like the proteins of other coatomer complexes (clathrin, COPI, and COPII), the proteins of the Nup107–160 subcomplex are predicted to contain β-propellers and α-solenoids, either alone or in combination. Indeed, the amino-terminal domain of Nup133 has been shown to be a seven-bladed propeller (11). Proteins of the yeast Nup84 subcomplex have been expressed recombinantly in *Escherichia coli* and assembled into a Y-shaped complex (9).

Nuclear envelopes containing functional NPCs can be reassembled *in vitro* by incubating *Xenopus laevis* egg extracts with envelope-denuded sperm nuclei (12). When the Nup107–160 subcomplex is immunodepleted from these extracts, NPCs cannot be reassembled (13). In RNA interference experiments wherein Nup107 is depleted from HeLa cells, NPCs are still assembled *in vivo* albeit compromised in their function (14, 15). Although the assembly of most members of the Nup107–160 subcomplex is not affected by Nup107 depletion, the resulting NPCs lack Nup133 (15). The lack of the Nup107/Nup133 dimer prevents the assembly of the asymmetric Nup214 and Nup358 on the cytoplasmic side and Nup153 on the nucleoplasmic side. Although these findings suggest that distinct members of the Nup107–160 subcomplex mediate specific interactions to other Nups and Nup subcomplexes, it remains to be determined how the nuclear envelope of higher eukaryotes disassembles and the NPCs disintegrate into distinct subcomplexes. Because the mitotic disassembly of NPCs is likely to be driven by reversible phosphorylation of a subset of Nups, which disrupts structurally significant Nup interactions, it is critical to determine where and when these Nups are phosphorylated.

A number of Nups are phosphorylated at mitosis (4–6, 16, 17). A recent study using temperature-sensitive Cdk1 *Drosophila* embryos showed that Cdk1 activity is required for keeping NPCs dissociated during mitosis, while the reassembly may be phosphatase-dependent (18). The goal of the present study is to map and characterize the cell-cycle-dependent phosphorylation of the main components of the Nup107–160 subcomplex to throw light on the regulation of disassembly and reassembly of the NPC. We found 12 phosphorylated residues that were present within the four higher molecular weight members of the Nup107–160 subcomplex that allow us to distinguish between several G_1 and mitotic events. These phosphorylated residues were localized in regions of the Nup107–160 proteins, which are predicted to be natively disordered.

Author contributions: J.S.G., A.N.K., I.M.C., T.B., G.B., and B.T.C. designed research; J.S.G., A.N.K., I.M.C., and T.B. performed research; J.S.G. and T.B. contributed new reagents/analytic tools; J.S.G., A.N.K., I.M.C., I.C.B., and B.T.C. analyzed data; and J.S.G., I.M.C., I.C.B., G.B., and B.T.C. wrote the paper.

The authors declare no conflict of interest.

Abbreviations: NPC, nuclear pore complex; Nup, nucleoporin.

‡Present address: Department of Pharmaceutical Chemistry, University of California, San Francisco, CA 94143.

§To whom correspondence may be addressed. E-mail: blobel@rockefeller.edu or chait@rockefeller.edu.

This article contains supporting information online at www.pnas.org/cgi/content/full/0700058104/DC1.

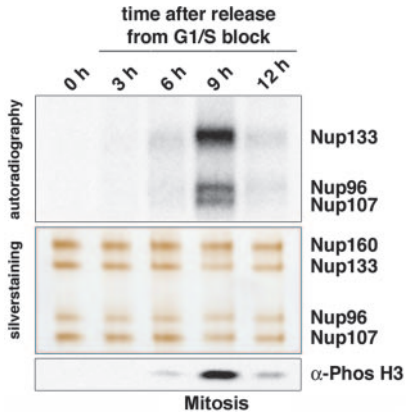

Fig. 1. Members of the Nup107–160 subcomplex are phosphorylated during mitosis. Cells were synchronized by using a double thymidine block and incubated in ^{32}P for 2 h before collection at the indicated time points. The resulting cell lysates were used for immunoprecipitation with affinity-purified α-Nup107 antibodies. The immunoprecipitated proteins were separated on 6% gels and analyzed by autoradiography (*Top*) and silver staining (*Middle*). Progression through the cell cycle was monitored by immunoblotting using anti-phospho-histone H3 (Ser-10) antibodies as a mitotic marker (*Bottom*).

Results and Discussion

Immunoisolation of the Nup107–160 Subcomplex at G_1 and Mitosis. The correct synchronization of HeLa cells was ensured by using classical approaches of double thymidine block and ^{32}P labeling. We chose not to add mitotic arresting agents such as nocodazole or taxol to avoid potential adverse consequences of their activities. Such agents change the dynamics of microtubules and hence may affect the distribution of kinases within the cell. After the double thymidine block, cells were harvested and lysed at various time points, and the subcomplex was immunoisolated by using affinity-purified α–Nup107 antibodies. The immunoprecipitated proteins were separated by using a 6% SDS/PAGE gel to yield optimal separation of four major components of the Nup107–160 subcomplex (Nup160, Nup133, Nup96, and Nup107; Fig. 1). The gels were silver-stained, demonstrating equal loading of the samples (Fig. 1 *Middle*), and autoradiographed to detect phosphorylation levels (Fig. 1 *Top*). The ^{32}P labeling (Fig. 1 *Top*) shows that only Nup133, Nup107, and Nup96 were radio-labeled, whereas Nup160 was not. As a mitotic marker, we used antibodies against histone H3 phosphorylated on Ser-10 (Fig. 1 *Bottom*), which reached a maximum at 9 h after the release from the thymidine block (Fig. 1 *Bottom*).

Based on the results in Fig. 1, we used cells harvested at the 0-h time point to represent those in G_1 and cells at the 9-h time point to represent those in mitosis. The cells from these two time points were lysed, and the Nup107–160 subcomplex was isolated by immunopurification via the α–Nup107 antibodies. The immunoprecipitates were resolved on 4–20% gradient gels and subsequently silver-stained (Fig. 2). MS analyses confirmed the presence of all nine members of the Nup107–160 subcomplex. It is noteworthy that we identified an isoform of Nup96 from the Nup98–96 precursor (Nup 98 isoform 1; GenBank accession no. NP057404.2) that contains an additional 88 amino acids at the C terminus (predicted to be natively disordered). The MS analysis covered >70% of the sequence for each of the four highest molecular weight protein components of the Nup107–160 subcomplex [supporting information (SI) Table 3 and SI Fig. 7].

Mapping Phosphorylation Sites on Nup160, Nup133, Nup96, and Nup107. We mapped the phosphorylation sites on Nup160, Nup133, Nup96, and Nup107 in mitotic cells by using a systematic multistage MS approach (MS, MS^2, MS^3) (19). Immunoprecipitation with the α-Nup107 antibodies was performed from 5×10^8 cells to obtain sufficient amounts of protein. After single-stage MS analysis, every discernable peptide ion peak above background was marked for analysis for phosphorylation. These peptide ions were analyzed in the MS^2 mode for the loss of 98 Da, the signature cleavage of the elements of phosphoric acid (H_3PO_4) from phosphorylated peptide ions (reviewed in ref. 20). Putative phosphorylation sites were then mapped to specific amino acids with MS^3 analysis by collision-induced dissociation of the $[M+H\text{-}H_3PO_4]^+$ ion. An example of this strategy is illustrated in Fig. 3 for the detection of Nup107 phosphorylation at Ser-37. The phosphorylation site was determined through consecutive MS, MS^2, and MS^3 analyses of pT_8, the phosphorylated counterpart of Nup107 T_8 peptide. In addition, we examined previously described sites of phosphorylation (17) with both a search for phosphorylated peptides at the MS level and a hypothesis-driven multiple-stage MS approach (19). This combined approach resulted in an average coverage of 84% for serines and 86% for threonines for the four Nups (SI Table 3). Gaps in MS coverage of the tryptic digests (SI Fig. 7) were the result of tryptic peptides with masses either <600 Da or >4,000 Da (i.e., outside the range of our instrumentation). Using this approach, we determined 11 distinct sites of phosphorylation within the four Nups and one site within Nup96 situated between residues 211 and 227 (Table 1).

A recent phosphoproteome analysis of the human mitotic spindle also detected the presence of certain phosphorylation sites on Nup160, Nup133, Nup96, and Nup107 (17), three sites

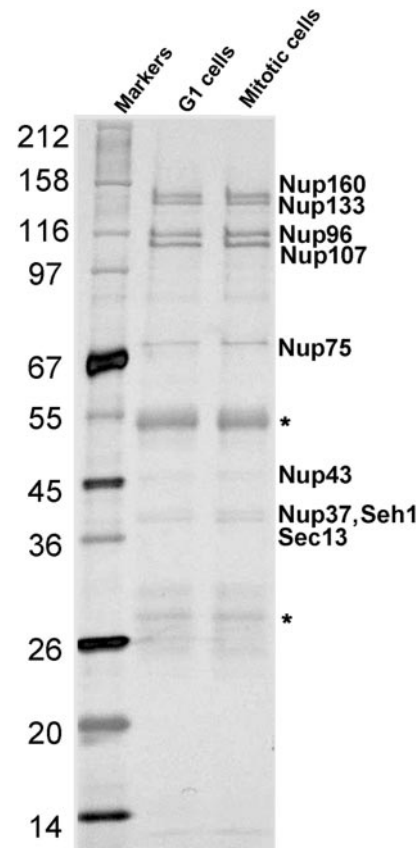

Fig. 2. Immunoprecipitation of the Nup107–160 subcomplex with affinity-purified α-Nup107 antibodies. Immunoprecipitated proteins were separated on a 4–20% gradient gel and stained with either silver (shown) or zinc (used for MS analysis). G_1 cells were collected immediately after the double thymidine block, whereas mitotic cells were collected 9 h after release from double thymidine block. *, IgG chains.

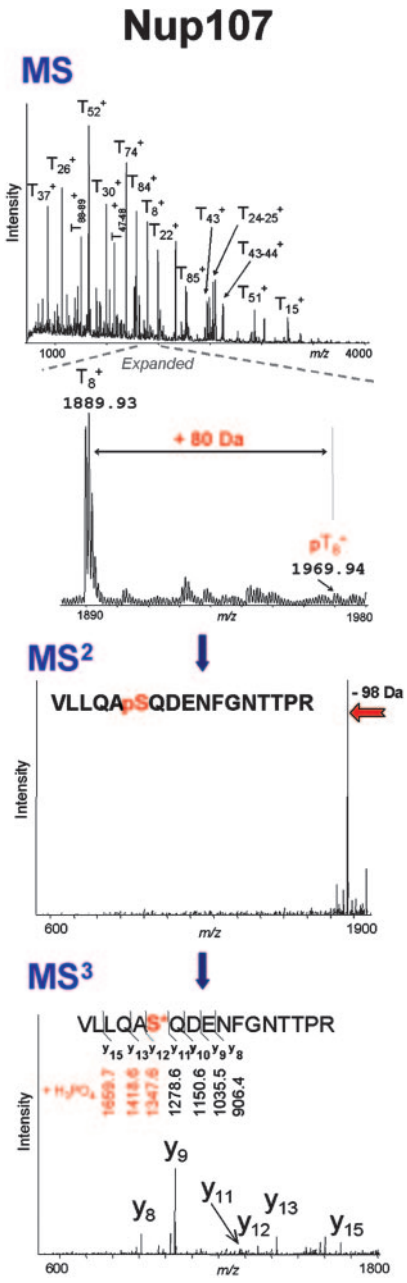

Fig. 3. Mapping the phosphorylation site at Ser-37 of Nup107 by MS, MS^2, and MS^3 analyses. (*Top*) MALDI-Qq-ToF MS (mass fingerprint) analysis of tryptic peptides (T_i) derived from Nup107, and expanded view of peptide T_8^+ at 1889.93 *m/z* and its phosphorylated counterpart pT_8^+ at 1969.94 *m/z*. Phosphate incorporation adds 80 Da. (*Middle*) MALDI-ion trap MS^2 (product ion spectrum) of the phosphorylated $[M+H]^+$ T_8 peptide (VLLQASQDENFGNTTPR) obtained by collision-induced dissociation. The characteristic loss of 98 Da, equivalent to H_3PO_4, is shown. (*Bottom*) MALDI-ion trap MS^3 of the $[M+H-98]^+$ ion identifying the site of phosphorylation at Ser-37 of Nup107 (VLLQApSQDENFGNTTPR). S* corresponds to dehydroalanine (i.e., phosphoserine has lost a phosphate group plus water).

of which are the same as those observed in the present study (Nup160 S1157, Nup133 S45, and Nup107 S11). We did not detect the other reported sites (17) with our highly sensitive hypothesis-driven multiple-stage MS approach (although we readily observed the corresponding unphosphorylated peptides). The induction of mitosis in the reported human mitotic spindle isolation study (17) involved the use of microtubule-specific drugs, namely nocodazole and taxol, to maximize yield. It is possible that their presence may lead to misplaced kinase activity. We also cannot eliminate the possibility that the subpopulation of Nups that was isolated with the mitotic spindle may be enriched for a different set of phosphorylation sites. In this context, it is noteworthy that we identified nine phosphorylation sites that have not been previously described to our knowledge.

Clustering of Phosphorylation Sites on Predicted Natively Disordered Domains. The majority of the detected phosphorylation sites on Nup133, Nup107, and Nup96 were confined to their N-terminal portions. Of the 12 phosphorylation sites mapped in this study, only one phosphothreonine was detected; the others were phosphoserines. Fig. 4 indicates the location of these phosphorylation sites relative to structural domains predicted by the algorithm PONDR (reviewed in ref. 21). We observed that the phosphorylation sites map exclusively to the predicted natively disordered regions of these proteins, including Nup160 (S1157), which is in a natively disordered region within its solenoid fold, and Nup96 (S894), which is C-terminal. All other phosphorylation sites mapped to the N-terminal disordered regions adjacent to the β-propeller of Nup133 (11) and the predicted α-solenoids of Nup96 and Nup107.

Natively disordered polypeptides often afford low-affinity, high-specificity interactions because of the balance of the binding energy with the entropic penalty paid during the disorder–order transition of binding. Additionally, because of their unstructured nature, these regions would be accessible to enzymatic activities that could drastically alter this energy balance, making regulation an easily attainable property. Phosphorylation of these areas suggests their possible involvement in interactions critical to NPC organization. The details of these interactions are currently unknown, although it has been proposed that helical solenoid domains in the subcomplex may represent binding domains between Nups (10). This proposal is supported by the Nup107–133 interaction, which was observed to occur through their helical solenoid domains (11). The β-propeller domains and disordered regions, in combination or individually, may then be responsible for anchoring Nups and hence the subcomplex within the NPC. In this case, the natively disordered regions would be prime targets for regulation.

For Nup133, the position of S76 presents interesting possibilities for the consequences that phosphorylation may have on Nup interactions. Based on the crystal structure, S76 precedes a tight β-turn at the junction between its disordered N terminus and the β-propeller (11). Phosphorylation of this residue will likely alter this structure and could provide a conformational switch for regulation of a protein–protein interaction. Disruption of the β-turn could mask or expose a binding site along the β-propeller's lateral surface (11). Additionally, the N-terminal disordered region of Nup96 was shown to interact with Sec13, a β-propeller protein and member of the Nup107–160 subcomplex (22). Sec13 is also a member of the COPII coat, and structural data suggest it forms the vertices of the COPII coat cage (23). If Sec13 played a similar role in the NPC, it may mediate inter-Nup107–160 subcomplex interactions whose regulation might be important for NPC disassembly. It remains to be seen whether the phosphorylation sites within the Nup96 N-terminal region overlap and/or affect its interaction with Sec13.

Relative Quantification of Phosphorylation Levels at G_1 and Mitosis. To study the cell-cycle dependence of the identified phosphorylation sites, we designed a method to quantify the relative levels of phosphorylation in G_1 versus mitotic cells (Fig. 5). Our strategy uses metabolic heavy isotope labeling, followed by immunoisolation of the Nup107–160 subcomplex, resolution of the protein constituents by SDS/PAGE, and MS readout of changes in site-specific phosphorylation. Although ^{32}P labeling is useful for surveying the phosphorylation status of specific

CELL BIOLOGY

Table 1. Phosphorylation sites of Nup160, Nup133, Nup96, and Nup107 detected by multiple-stage MS (MS, MS^2, MS^3)

Protein	Tryptic peptide	Phosphorylation sites
Nup160	^{1134}LIRPEYAWIVQPVSGAVYDRPGA**pS**PK^{1159}	S1157*
Nup133	^{35}KGLPLGSAVS**pS**PVLF**pS**PVGR^{54}	S45* and S50
Nup133	^{67}MFPHHSITEpSVNYDVK^{82}	S76
Nup96	^{1}SKYGLQDSDEEEEEHPSKT**pS**TK^{21}	S19
Nup96	^{25}TAPLPPA**pS**QT**pT**PLQMALNGKPAPPPQSQSPEVEQLGR^{61}	S32 and T35
Nup96	^{193}AASLMNIPSTSSWSVPPPLT**S**VF**T**MP**S**PAPEVPLK^{227}	Region 211–227†
Nup96	^{877}VVLSLHHPPDRTSD**pS**TPDPQRVPLR^{901}	S891
Nup107	^{4}SGFGEIS**pS**PVIR^{15}	S11*
Nup107	^{32}VLLQA**pS**QDENFGNTTPR^{48}	S37
Nup107	^{119}SGLFTNTEPH**pS**ITEDVTISAVMLR^{142}	S129

Phosphorylated residues are highlighted in bold.
*Previously identified sites (17).
†Exact residue undetermined.

proteins under cell-cycle-dependent conditions, the technique is subject to certain limitations. In particular, active turnover of phosphorylated amino acids is a prerequisite for radiolabel incorporation during a short exposure to the radioactive precursors (≈2 h). Under these conditions, sites that are constitutively phosphorylated may not be detected. By contrast, the MS readout relies only on the presence of a phosphorylated residue, not its turnover rate.

As illustrated in Fig. 5, we metabolically labeled G_1 cells with a form of either isotopically heavy Lys ([U-$^{13}C_6$]-L-lysine) or heavy Arg ([U-$^{13}C_6$,$^{15}N_4$]-L-arginine) and mixed them with an equal number of unlabeled mitotic cells. Under the growth condition used, the level of heavy Lys incorporation was 88%, yielding peptides from G_1 cells with masses increased by 6 Da over those generated from mitotic cells (SI Table 4). The mixing ratio of immunoaffinity-purified Nup107–160 subcomplex from G_1 and mitotic cell lysates was measured to be close to one-to-one (SI Table 5). Given sufficient signal-to-noise, single-stage MS analysis can provide accurate measures of the relative levels of the G_1 and mitotic peptides. However, because most of the detected phosphopeptides had relatively low signal-to-noise ratios, we determined the relative quantifications at the MS^2 level. In these experiments we measured the ratio of site-specific phosphorylation from the G_1 (labeled) and mitotic (unlabeled) phosphopeptide ions by using the pair of predominant −98-Da fragment ion peaks. We have shown previously that quantitation using these phosphopeptide fragmentation ions yields accurate relative abundance ratios because of the improved signal-to-noise ratio in the MS^2 spectra (24).

Fig. 6 shows examples of our results for the quantitative MS analysis of the phosphorylation of Nup133 and Nup160. The ratios of fragment ions of unphosphorylated peptides from these Nups (Fig. 6 *Bottom*) provided accurate normalizations between the level of isolated proteins from the G_1 and mitotic stages. The results are summarized in Table 2. The M/G_1 ratio for Nup160 phosphorylated at S1157 was 1.08 ± 0.06, consistent with the ratio expected for constitutive phosphorylation of this site, explaining its lack of visualization by ^{32}P labeling (Fig. 1). Constitutive phosphorylation was also observed for Nup96, with

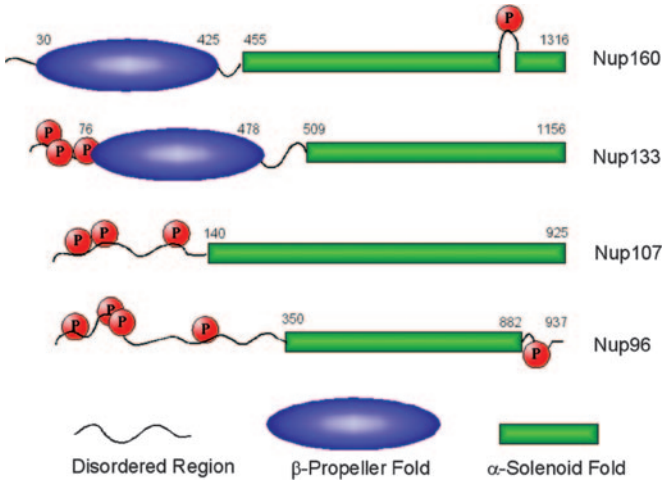

Fig. 4. Domain structures of the high-molecular-weight components of the Nup107–160 subcomplex: Nup160, Nup133, Nup96, and Nup107. The sites of phosphorylation are shown as red spheres located within the curved black lines signifying predicted natively disordered regions. β-Propellers are shown as blue ellipses, and α-solenoids are shown as green bars.

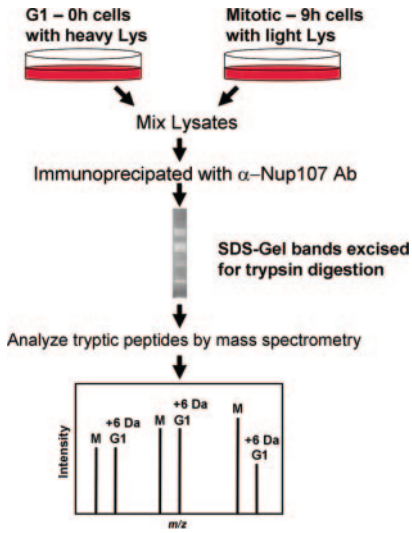

Fig. 5. Method for relative quantification of cell-cycle-dependent phosphorylation using metabolic isotopic labeling. G_1 HeLa cells were grown in media with heavy lysine ([U-$^{13}C_6$]-L-lysine, +6 Da). The isotopically heavy G_1 lysate was mixed in equal proportion with lysate from the mitotic population of HeLa cells, grown in isotopically light lysine media. The Nup107–160 subcomplex was immunoprecipitated from the mixture with affinity-purified α–Nup107 antibodies, resolved by SDS/PAGE, and analyzed by MS. MS analysis reveals pairs of peptides, separated by 6 Da, corresponding to the M and G_1 states. In the schematic spectrum shown for illustration purposes, the ratios between the heights of the M and G_1 peaks yield the relative protein levels (two left pairs of peaks) and phosphorylation levels (right peak).

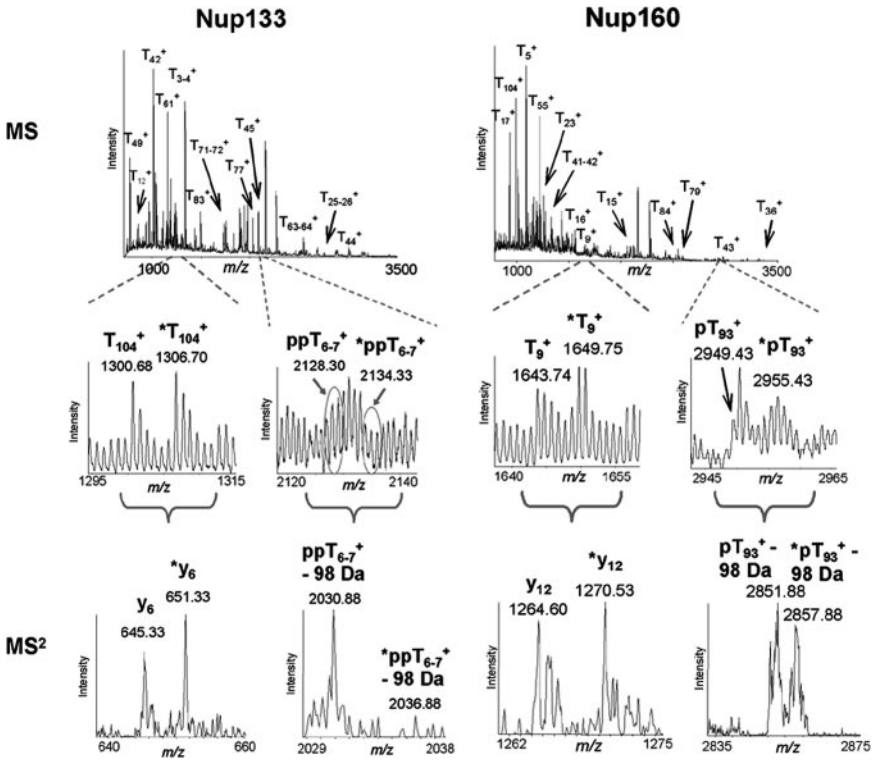

Fig. 6. Comparison of phosphorylation levels at G_1 and mitosis for Nup133 (S45 and S50) and Nup160 (S1157). (*Top*) Single-stage mass spectra of tryptic digests Nup133 (*Left*) and Nup160 (*Right*). T_i denotes the *i*th tryptic peptide. (*Middle*) Expanded view of indicated light and heavy unphosphorylated and phosphorylated tryptic peptides. ppT_i denotes a doubly phosphorylated peptide, and pT_i indicates a singly phosphorylated peptide. (*Bottom*) Two-stage mass spectra (MS^2) of the indicated light and heavy unphosphorylated and phosphorylated tryptic peptides. The M/G_1 ratio for Nup133 ppT_{6-7} (containing phosphorylated S45 and S50; Table 2) is 12.5 ± 1.8, clearly indicating mitotic phosphorylation. The M/G_1 ratio for Nup160 pT_{93} containing phosphorylated S1157 (Table 2) is 1.08 ± 0.06, indicating constitutive phosphorylation.

M/G_1 ratios of 0.8 ± 0.05 for S19 and 1.2 ± 0.3 for S32 and/or T35. We were not able to quantify the remaining sites on Nup96 (Table 1) because of the limited mass range of our multiple-stage mass spectrometer. However, we think it likely that one or more of these Nup96 sites may undergo mitotic-directed modification. Nup133 exhibited a high degree of mitotic-specific phosphorylation with the S45+S50 (double phosphorylation) and S76 sites having M/G_1 ratios of 12.5 ± 1.8 and 6.1 ± 1.3, respectively. Nup107 S11 had an M/G_1 ratio of 4.9 ± 1.4, also indicating increased phosphorylation during mitosis. These MS quantification results confirm the mitotic-dependent phosphorylation of the Nups seen in Fig. 1 using ^{32}P labeling, yielding significant site-specific changes as a function of the cell-cycle state.

Conclusions

For more than a decade, mitotic disassembly of the NPC has been speculated to be driven largely by reversible phosphorylation of a subset of Nups (4–6). However, the specific phosphorylated sites were unknown and much remains to be elucidated about the regulators that control the disassembly of the NPC. Nup107–160 subcomplexes are made up of helical solenoids, well suited for interactions with multiple partners, and compact stable repeat structures, such as β-propellers, ideal for forming reversible interactions (10, 11). In addition, several members of the subcomplex contain large regions predicted to be natively disordered. We find it intriguing to speculate that Nup107, and potentially Nup96 and Nup133, represent anchoring points of the Nup107–160 subcomplex within the NPC by interacting with adjoining Nups and Nup subcomplexes. Phosphorylation at key sites on these anchoring proteins may alter interactions and therefore aid the release of peripheral Nups and the subcomplex from the NPC.

Our study describes the cell-cycle dependency of phosphorylation events on Nup160, Nup133, Nup96, and Nup107, the high-molecular-weight members of the Nup107–160 subcomplex. The high specificity of MS methods has enabled us to map and quantify the level of Nups phosphorylation *in vivo* at the different cell-cycle stages. Our systematic multistage MS approach proved to be an effective method for detecting and quantifying phosphopeptides. This study represents a comprehensive examination of the phosphorylation of Nups in the NPC. Starting with isolation of the entire subcomplex in G_1 and mitosis from HeLa cells, we identified 12 phosphorylated residues that were present within the Nup107–160 subcomplex. These phosphorylated residues cluster within unstructured regions of Nups, which may result in conformational changes that regulate their interactions. An example is S76 of Nup133, which was shown in the crystal structure to precede a tight β-turn at the N terminus of the β-propeller domain (11). The present results provide the basis for future studies into details of the mechanism for NPC assembly and disassembly during the cell cycle.

Table 2. Relative quantification of phosphorylation levels at G_1 and M cell-cycle stages

Protein	Site	M/G_1 ratio
Nup160	S1157	1.08 ± 0.06
Nup133	S45 and S50	12.5 ± 1.8
Nup133	S76	6.1 ± 1.3
Nup96	S19	0.8 ± 0.05
Nup96	S32 and T35	1.2 ± 0.3
Nup107	S11	4.9 ± 1.4

CELL BIOLOGY

Methods

Antibody Production. To raise polyclonal antibodies against human Nup107, recombinant GST-Nup107 (amino acids 101–165) was injected into rabbits, and sera were collected after an appropriate response had been elicited (Colcalico Biologicals, Inc., Reamstown, PA). The α–Nup107 antibodies were affinity-purified as described by using recombinant protein immobilized on nitrocellulose membrane (22).

Immunoprecipitation. Immunoprecipitation was performed as described (25) with some modifications, namely the addition of phosphatases inhibitors (50 nM calyculin A, 25 mM sodium fluoride, phosphatase mixture inhibitor I and II from Sigma, St. Louis, MO) in the buffer. After the final wash, the protein A-Sepharose pellet was suspended in 1× SDS-sample buffer, products were resolved by SDS/PAGE using either a 6% or a 4–20% Tris-glycine gel (Novex; Invitrogen, Carlsbad, CA), and visualized either by silver staining (SilverXpress, Invitrogen) or zinc staining for MS analysis (Bio-Rad, Hercules, CA).

Cell-Cycle Synchronization and *in Vivo* Labeling. HeLa cells, grown in DMEM (Invitrogen) supplemented with 10% FBS, penicillin, and streptomycin, were synchronized by using a double thymidine block. Progression through the cell cycle was monitored by immunoblotting with anti-phospho-histone H3 (Ser-10) antibodies (Upstate Biotechnology, Lake Placid, NY) as a mitotic marker. For *in vivo* labeling with ^{32}P, cells were washed and incubated for 30 min in phosphate-free DMEM (Invitrogen) supplemented with 5% FBS. Subsequently, the medium was replaced with phosphate-free DMEM containing 200 μCi/ml of inorganic [^{32}P]ortho-phosphoric acid, incubated in ^{32}P for 2 h before collection at each indicated time point.

Analysis of Nups Phosphorylation by Multiple-Stage MS. Protein in-gel digestion and extraction from gel bands were performed as described (26). Mass spectra were collected with an in-house-built MALDI interface coupled to either a QqToF instrument (QqTOF Centaur; Sciex, Concord, ON, Canada), used for peptide fingerprinting (MS), or an ion trap (LCQDECAXP^{PLUS}; Finnigan, San Jose, CA), for amino acid sequence analysis (MS^2, MS^3) (26, 27). A vacuum-MALDI ion trap (vMALDI LTQ; Finnigan) was also used for the latter analyses. Multiple-stage MS (MS^2, MS^3) and computer analyses have been described (19, 26–28).

Relative Quantification of Phosphorylation Sites by Stable Isotope Labeling (SILAC). SILAC (29) was performed on HeLa cells with a SILAC Protein ID and Quantitation kit (SP10001; Invitrogen). HeLa cells were grown in DMEM, minus Lys and Arg (Invitrogen), supplemented with 10% dialyzed FBS, penicillin, and streptomycin, and synchronized by using a double thymidine block. G_1 cells were grown in medium containing either heavy Lys ([U-$^{13}C_6$]-L-lysine, molecular mass of 152.126 Da, resulting in an increase of 6.020 Da in molecular mass), or heavy Arg ([U-$^{13}C_6$,$^{15}N_4$]-L-arginine, molecular mass of 184.124 Da, resulting in a 10.012 Da increase in molecular mass), and then lysed. An aliquot from each sample was used to measure the efficiency of label incorporation. The lysate was then mixed with an equal amount of lysate from unlabeled mitotic cells, and immunoisolations were performed by using the affinity-purified α-Nup107 antibodies. Protein in-gel digestion and extraction from gel bands were performed, and peptides were analyzed by MS (see above).

We thank Martin Kampmann, Sarah Whitcomb, Sam Dales, Ivo Melcak, Elias Coutavas, Jeff Degrasse, and Julio Padovan for support and helpful discussions. This work was supported by National Institutes of Health Grant RR00862 (to B.T.C.), The Rockefeller University Women and Science Fellowship CEN5300379 (to I.M.C.), and the Howard Hughes Medical Institute. J.S.G. was supported by National Institutes of Health Individual National Research Service Award 5F32GN20520.

1. Tran CW, Wente SR (2006) *Cell* 125:1041–1053.
2. Rout MP, Aitchison JD, Suprapto A, Hjertaas K, Zhao Y, Chait BT (2000) *J Cell Biol* 148:635–651.
3. Cronshaw JM, Krutchinsky AN, Zhang W, Chait BT, Matunis MJ (2002) *J Cell Biol* 158:915–927.
4. Macaulay C, Meier E, Forbes DJ (1995) *J Biol Chem* 270:254–262.
5. Favreau C, Worman HJ, Wozniak RW, Frappier T, Courvalin JC (1996) *Biochemistry* 35:8035–8044.
6. Bodoor K, Shaikh S, Salina D, Raharjo WH, Bastos R, Lohka M, Burke B (1999) *J Cell Science* 77:321–329.
7. Belgareh N, Rabut G, Bai SW, van Overbeek M, Beaudouin J, Daigle N, Zatsepina OV, Pasteau F, Labas V, Fromont-Racine M, *et al.* (2001) *J Cell Biol* 154:1147–1160.
8. Loiodice I, Alves A, Rabut G, Van Overbeek M, Ellenberg J, Sibarita JB, Doye V, Forbes DJ (2004) *Mol Biol Cell* 15:3333–3344.
9. Lutzmann M, Kunze R, Buerer A, Aebi U, Hurt E (2002) *EMBO J* 21:387–397.
10. Devos D, Dokudovskaya S, Alber F, Williams R, Chait BT, Sali A, Rout MP (2004) *PLoS Biol* 2:e380.
11. Berke IC, Boehmer T, Blobel G, Schwartz TU (2004) *J Cell Biol* 167:591–597.
12. Newmeyer DD, Finlay DR, Forbes DJ (1986) *J Cell Biol* 103:2091–2002.
13. Harel A, Orjalo AV, Vincent T, Lachish-Zalait A, Vasu S, Shah S, Zimmerman E, Elbaum M, Forbes DJ (2003) *Mol Cell* 11:853–864.
14. Walther TC, Alves A, Pickersgill H, Loiodice I, Hetzer M, Galy V, Hulsmann BB, Kocher T, Wilm M, Allen T, *et al.* (2003) *Cell* 113:195–206.
15. Boehmer T, Enninga J, Dales S, Blobel G, Zhong H (2003) *Proc Natl Acad Sci USA* 100:981–985.
16. Beausoleil SA, Jedrychowski M, Schwartz D, Elias JE, Villen J, Li J, Cohn MA, Cantley LC, Gygi SP (2004) *Proc Natl Acad Sci USA* 101:12130–12135.
17. Nousianinen M, Sillje HH, Sauer G, Nigg EA, Korner R (2006) *Proc Natl Acad Sci USA* 103:5391–5396.
18. Onischenko EA, Gubanova NV, Kiseleva EV, Hallberg E (2005) *Mol Biol Cell* 16:5152–5162.
19. Chang EJ, Archambault V, McLachlin DT, Krutchinsky AN, Chait BT (2004) *Anal Chem* 76:4472–4483.
20. McLachlin DT, Chait BT (2001) *Curr Opin Chem Biol* 5:591–602.
21. Dunker AK, Brown CJ, Lawson JD, Iakoucheva IM, Obradovic Z (2002) *Biochemistry* 41:6573–6582.
22. Enninga J, Levay A, Fontoura BM (2003) *Mol Cell Biol* 23:7271–7284.
23. Stagg SM, Gurkan C, Fowler DM, LaPointe P, Foss TR, Potter CS, Carragher B, Balch WE (2006) *Nature* 439:234–238.
24. Jin M, Bateup H, Padovan JC, Greengard P, Nairn AC, Chait BT (2005) *Anal Chem* 77:7845–7851.
25. Grandi P, Dang T, Pane N, Shevchenko A, Mann M, Forbes D, Hurt E (1997) *Mol Biol Cell* 8:2017–2038.
26. Krutchinsky AN, Kalkum M, Chait BT (2001) *Anal Chem* 73:5066–5077.
27. Krutchinsky AN, Zhang W, Chait BT (2000) *J Am Soc Mass Spectrom* 11:493–504.
28. Kalkum M, Lyon GJ, Chait BT (2003) *Proc Natl Acad Sci USA* 100:2795–2800.
29. Ong SE, Blagoev B, Kratchmarova I, Kristensen DB, Steen H, Pandey A, Mann M (2002) *Mol Cell Proteomics* 1:376–386.